International Journal of Mass Spectrometry 296 (2010) 59–64

Contents lists available at ScienceDirect

International Journal of Mass Spectrometry

journal homepage: www.elsevier.com/locate/ijms

Ion kinetic energy measurements in two soft ion ejection methods from a quadrupole ion trap

Maria A. van Agthoven[a,1], Philippe Colomby[a], Michel Surugue[a], Claude Beaugrand[b], Franck L. Wind[c], Jean-Claude Tabet[a,*]

[a] Laboratoire de Chimie Structurale Organique et Biologique, Université Pierre et Marie Curie – Paris 6, UMR 7613, Paris F-75 005, France
[b] ALPHA MOS, 20, Avenue Didier Daurat, F-31400 Toulouse, France
[c] Centre d'Etudes du Bouchet, BP No. 3, F-91710 Vert-Le-Petit, France

ARTICLE INFO

Article history:
Received 29 December 2009
Received in revised form 26 August 2010
Accepted 30 August 2010
Available online 9 September 2010

Keywords:
Quadrupole ion trap
Instrumentation
Kinetic energy
Ion ejection
Retarding grid analyzer

ABSTRACT

The kinetic energy of ion beams upon ejection from a quadrupole ion trap was measured in view of coupling quadrupole ion traps with other mass analyzers. Measurements were performed using a retarding grid analyser for two modes of ion ejection from the quadrupole ion trap based on the decrease of the amplitude of the radiofrequency voltage on the ring electrode simultaneously combined with the application of: (i) a positive voltage on the ring electrode and (ii) a voltage between the end-cap electrodes. We show that ion kinetic energy at ejection depends on the DC ejection voltage and the amplitude of the RF voltage at the moment of ejection, which means that the kinetic energy of the ions that are ejected from the ion trap depends on the m/z ratio. Ion focusing depends on the depth of the pseudo-potential well in the quadrupole ion trap.

1. Introduction

Increasingly, quadrupole ion traps (QIT) are being used in hybrid tandem mass spectrometers. They bring many advantages to instrumental performance, like ion accumulation for greater sensitivity, ion isolation and sequential MS^n possibilities [1]. One such hybrid tandem mass spectrometer is the QIT/TOF, which combines the properties of the QIT with the high resolution, accurate mass measurements and wide mass range of TOF-MS technology [2]. QIT/TOF hybrids have been built in linear configurations [3–7], using both pulsed and continuous ion sources like MALDI [8] and ESI [9], and couplings with liquid chromatography [10]. Commercial instruments are also available, like the AXIMA-QIT from Shimadzu, which has a MALDI [11] and an ESI ion source [12]. More recently, orthogonal couplings between QITs and TOF analyzers have been developed in order to take advantage from the gain in resolution that this configuration can bring [13]. A commercial instrument with high resolving power and mass accuracy using this configuration has been proposed by Hitachi [14,15].

Among the most important issues to overcome in order to successfully couple a QIT and a TOF analyzer is ion ejection from the QIT and transmission into the TOF push–pull zone. When the QIT is used alone as a mass analyzer, ions are resonantly ejected at the intersection of the $a_z = 0$ and $\beta_z = 1$ or $\beta_z = 2/3$ lines characterizing the stability diagram [16,17]. Ions are ejected from the QIT from low to high m/z ratios [1]. If ions that have been ejected in this way subsequently go through transfer optics, the time-of-flight difference between ions of high m/z ratio and ions of low m/z ratio increases even more than if ions are ejected simultaneously from the QIT. If the ions enter the push-pull zone of a TOF, the effective m/z range that is analyzed in the TOF is very small, because ions are pushed simultaneously in the drift zone [18]. Ejecting ions at the intersection of the $a_z = 0$ and $\beta_z = 1$ or $\beta_z = 2/3$ lines is therefore incompatible with an efficient operation of the TOF analyzer. Ejecting the ions by decreasing order of m/z ratios is better, so that the time-of-flight effect compensates for the ejection time of the ions from the QIT.

Furthermore, during the analytical scan of the QIT, ions are ejected at high RF and their kinetic energy is therefore very high [19]. This is unsuitable for injection into the TOF drifting tube, because high kinetic energy for orthogonally injected ions has negative impacts on the final performance of the instrument: the kinetic energy associated with the part of the ion motion in the z-axis of the QIT and the ion guide (i.e., orthogonally to the axis of the TOF drift-tube) has a negative effect on the sensitivity of the instrument, and the kinetic energy associated with the part of the ion

* Corresponding author. Tel.: +33 1 44 27 31 12; fax: +33 1 44 27 38 43.
E-mail address: jean-claude.tabet@upmc.fr (J.-C. Tabet).
[1] Present address: Laboratoire de Chimie Organique et Macromoléculaire, bat C4, Université des Sciences et Technologies de Lille, F-59655 Villeneuve d'Ascq cedex, France.

1387-3806/$ – see front matter © 2010 Elsevier B.V. All rights reserved.
doi:10.1016/j.ijms.2010.08.026

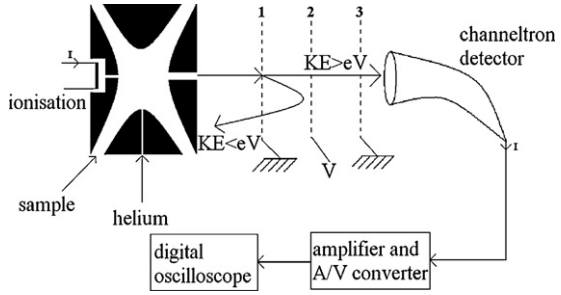

Fig. 1. Experimental setup and design of the retarding field analyzer.

motion orthogonally to the *z*-axis of the QIT (i.e., in axis with the TOF drift tube) has a negative effect on the resolving power of the TOF analyzer [20]. Although the kinetic energy associated with the ion motion in the axis of the drift tube is not an issue that can be ignored, its effect can be successfully compensated with a reflectron. Furthermore, in orthogonal couplings between QITs and TOF analyzers, the ions are injected in the push-pull zone of the TOF orthogonally to the drift tube axis. The kinetic energy associated with the part of the ion motion that is in the axis of the drift tube is therefore negligible compared with the kinetic energy associated with the part of the ion motion that is orthogonal to the drift tube.

In order to minimize the kinetic energy that is orthogonal to the drift tube, it is important to eject ions from the QIT at RF voltages in the regions of the stability diagram with low a_z and q_z values, where the ions' kinetic energy is lower because the pseudo-potential well is shallower. Since mass analysis at low a_z and q_z is inaccurate, this is not a common ejection method. As a result, there has historically not been a lot of interest in it. For this purpose, the behaviour of ions when they are ejected from the QIT is investigated in two ways, both involving a gradual decrease of the radiofrequency voltage amplitude on the ring electrode of the QIT. In one method, the ion ejection is enhanced by the application of a voltage on the ring electrode, and in the other method, by a voltage on the end-cap electrodes of the QIT. We present the results in terms of how the ion behaviour and kinetic energy when trapping parameters are changed.

2. Experimental methods

2.1. The retarding field analyzer

The retarding field analyzer (RFA) was designed by Simpson [21] in order to measure the kinetic energy of an ion or the kinetic energy distribution of an ion cloud. A device made of three parallel grids is placed between the ion optics and the detector, as is shown in Fig. 1. Energy conservation, which, in the context of electrostatics, states that the kinetic energy variation of a charged particle between two points of its trajectory is equal to the electric potential variation between those points, is used to determine the kinetic energy of particles arriving on the grids.

The principle of the RFA method is to discriminate ions according to their kinetic energy. The two outer grids of the device (grids 1 and 3 in Fig. 1) are at the same potential as the electrode in front of the device to avoid kinetic energy variations caused by the RFA. On grid 2 a repulsive voltage *V* is applied. Therefore, particles with an electric charge *Ze* and an initial kinetic energy lower than *ZeV* will not overcome the potential barrier created by the grids and will turn around. They will not reach the detector. Charged particles with an initial kinetic energy higher than *ZeV* will be able to overcome the potential barrier and reach the detector, as is displayed in Fig. 1. The ion current is measured for an increasing voltage on grid 2. The opposite of the derivative of the plot of the number of ions *vs*. the potential energy *ZeV* between grid 1 and 2 yields the initial kinetic energy of the charged particle. In the case of an ejected ion cloud, it will yield the kinetic energy distribution within the ion beam.

This method enables the measurement of accurate kinetic energy distributions regardless of the direction of ion trajectories. The use of grids ensures that electric potentials are properly defined as long as they are of good quality. The response from the detector is proportional to the ion abundance for the considered scale of kinetic energies, so that the ion signal can be used to measure the ion beam kinetic energy distribution.

The retarding field analyzer is a robust method that is still used in various applications, like the study of the energy distribution of negative carbon ion beams extracted from a plasma-splutter-type negative ion source [22] or of space charge-dominated electron beams [23]. It was also used to measure the kinetic energy of ions exiting the Omegatron RF cavity of the Alcator C-mod tokamak [24] and the JET plasma boundary [25].

2.2. Experimental setup

The experimental setup is shown in Fig. 1. The QIT was a modified SATURN™ III GC/MS from Varian (Walnut Creek, CA, USA) with EI/CI ionisation. The GC part of the sample inlet was removed. The sample was introduced through the calibration sample inlet by vapour tension of the liquid and ionized using EI. The voltages on the various electrodes and the operating voltage of the detector were controlled with QISMS™ version 1.0 software (Quadrupolar Ion Storage MS Scan Editor) [26]. This software allows the user to add temporal segments before the analytical mass scans with user-defined RF and DC voltages on the ring electrode, various waveforms, axial modulation and DC voltages on the end-cap electrodes and operation of the detector [27].

The QISMS programs used for the ion manipulation experiment are presented in Fig. 2. The first segment was an ionisation period of 25,000 μs. Then the ion species of interest was isolated (segment 1, 2, 3), cooled (4, 5 in Fig. 2a and 4 in Fig. 2b) and ejected (5 in Fig. 2a

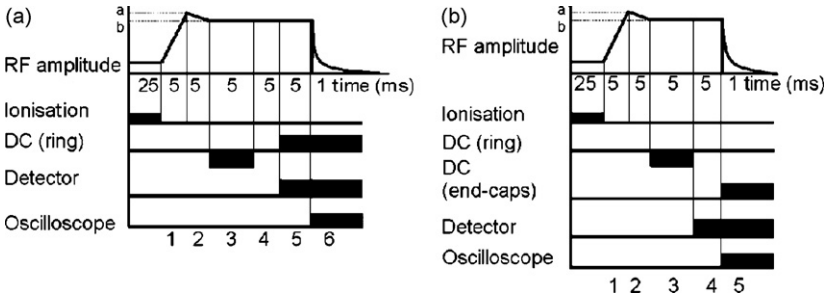

Fig. 2. QISMS programs for ejection of the ion cloud by simultaneous radiofrequency shut-down and (a) application of a DC voltage on the ring electrode or (b) application of a DC voltage between the end-cap electrodes. In both cases, there is an ionisation time of 25,000 μs, an isolation time (1, 2, 3), a cooling time (4, 5 for (a) and 4 for (b)) and an ejection time (6 for (a) and 5 for (b)).

and 6 in Fig. 2b). Shut-down of the radiofrequency voltage was combined with (a) a positive DC voltage on the ring electrode and (b) a DC voltage between the end-cap electrodes. Because of different rise times of the voltages, the DC voltage on the ring electrode was applied before the radiofrequency shut-down, while the DC voltage between the end-cap electrodes was applied simultaneously with the radiofrequency shut-down (this voltage is symmetric: in the rest of this study, when we refer to a voltage 2 V between the end-cap electrodes, this means that the voltage on the electrodes is +V and −V). The response of the amplitude of the radiofrequency voltage to a shut-down was exponential with a time constant of 200 μs which did not vary significantly with the initial amplitude of the radiofrequency.

Between the QIT and the detector, a retarding field analyzer constituted of three grids was placed. The voltages on the grids were controlled with a 410 V generator with a variable offset. The voltages on the grids were applied with a ±0.1 V accuracy.

The detector was an on-axis channeltron electron multiplier. The ion current was converted and amplified with a home-built fast amplifier (stable gain for signal frequencies over 1 MHz). The signal was measured by a Lecroy Waverunner 6050A digital oscilloscope (Lecroy France, Courtabœuf, France) with a 100 MS/s sampling rate and a 20 μs/div time scale. The data were further analyzed using Excel and Origin software.

The sample for this study is a perfluorotri-n-butylamine (FC-43) calibration sample purchased from Aldrich (Milwaukee, WI, USA). The fragment ion species studied were m/z 69, 131, 264, 414 and 502. For m/z 69, 131 and 264, the initial radiofrequency amplitude at ejection corresponded to the position of these ion species on the q_z axis at the apex position of the stability diagram. For m/z 414 and 502, the initial radiofrequency amplitude was lowered in order to avoid longer ejection times than the oscilloscope could store without changing the sampling rate.

For ion ejection by application of a DC voltage on the ring electrode, grids 1 and 3 were grounded. For application of a DC voltage between the end-cap electrodes, the voltage on grids 1 and 3 was taken to be equal to the voltage on the exit end-cap electrode. Therefore, there was no electric field between the exit end-cap electrode and the retarding field analyzer. The ion kinetic energy distribution was not altered after ejection from the QIT.

In order to measure q_z and a_z at ion ejection, the ejection time was measured by comparing the command of the radiofrequency drive and the signal peak in the absence of a retarding field. Then, the radiofrequency amplitude was calculated using the initial amplitude of the radiofrequency voltage and its exponential decrease. The values of q_z and a_z were then calculated using utilities of the QISMS software. This was only possible in the case of ejection by application of a DC voltage on the ring electrode, since it is only in that case that q_z and a_z are defined.

For the kinetic energy distribution, the ion signal was measured for increasing values of the voltage on grid 2, baseline-subtracted and summed using Excel in order to define ion intensity. For each point in the ion signal *vs*. voltage on grid 2 plot, the signal was averaged over 5 measurements in order to lessen the influence of signal fluctuations. The subsequent plot of ion intensity *vs*. voltage on grid 2 was further smoothed with a mobile 3 point average. The derivative was then calculated using the following equation:

$$D(ZeV_i) = \frac{I(V_i + \Delta V) - I(V_i)}{\Delta V}$$

where $D(ZeV_i)$ is the distribution of kinetic energy at $E_K = ZeV_i$, where the electric charge of the ions is Ze, the intensity measured at voltage V_i is $I(V_i)$, and the increase in voltage on grid 2 is ΔV.

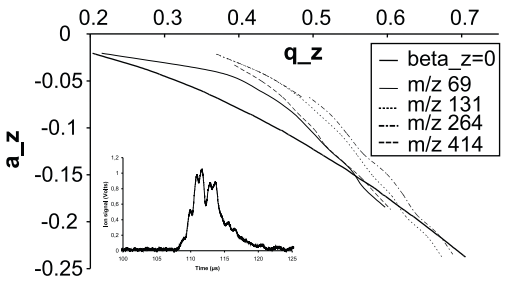

Fig. 3. Plot of the curve in the stability diagram after measurement of the ejection of several ion species by simultaneous radiofrequency shut-down and application of a DC voltage on the ring electrode and theoretical calculation.

3. Results and discussion

In the insert of Fig. 3, we can see an example of the signal of m/z 414 that was collected by the channeltron detector. The duration of the ion train is typically 5–10 μs. The signal shows local maxima that are roughly 1 μs apart. During ion ejection from the QIT, the radiofrequency is still applied to the ring electrode with a 1.05 MHz frequency. The local maxima in the ion signal suggests that ion ejection from the QIT depends on the phase of the RF voltage on the ring electrode, and that ions are preferentially ejected when the RF voltage is positive (i.e., ions are repulsed by the ring electrode).

In Fig. 3, we see the shift of the $\beta_z = 0$ boundary curve for the various ion species that were studied, using the application of a DC voltage on the ring electrode. We measured the time between the start of the exponential decay of the RF amplitude and the signal of the ions, which is an accurate measurement of the ejection time of the ions. Since we had previously determined the time constant of the decay of the RF amplitude, we calculated the RF amplitude at ion ejection using the following equation:

$$V_{RF}^{\text{ejection}} = V_{RF}^{\text{initial}} e^{t_{\text{ejection}}/\tau}$$

where V_{RF}^{initial} is the initial RF amplitude, V_{RF}^{ejection} is the RF amplitude at ejection, t_{ejection} is the ejection time of the ions and τ is the time constant of the exponential decay ($\tau = 200$ μs, as is indicated in the Experimental Setup section). Considering that the measurement of the ejection time is very steady (data not shown) and that the ion train is approximately 10 μs, the relative error for these calculations was estimated to be approximately 5%.

Using QISMS software, we were able to convert the RF amplitude and the DC voltage applied to the ring electrode in q_z and a_z for each data point. Since the Mathieu equations only apply to voltages on the ring electrode, thinking in terms of q_z and a_z values only makes sense when the DC voltage is applied on the ring electrode or when the same voltage is applied on both end-cap electrodes. When opposite DC voltages are applied on the end-cap electrodes, the ions remain on the $a_z = 0$ axis on the stability diagram. However, the stability diagram no longer accurately reflects the experimental conditions in the QIT.

In Fig. 3, we can see that the (q_z, a_z) values at which ions are ejected do not overlap with the theoretical $\beta_z = 0$ curve. There may be several reasons for this behaviour. The first one is the difference between the time of crossing the stability curve and the time of arrival of the ions on the detector, because the distance between the ion trap exit and the detector is 5 cm.

The second explanation involves space charge effect. It has been shown [28,29] that space charge induces a displacement of the stability diagram to the right in the (q_z, a_z) plane. The $\beta_z = 0$ curve is therefore shifted to the right. Although each ion species was isolated before ejection, we still measured a total ion current of several thousand ions. Since the fragment ions obtained by dissociation of the ionized FC-43 sample all have different abundances,

Table 1
Total intensity of the ions ejected from the ion trap by application of a DC voltage on the ring electrode, in arbitrary unit. The total ion intensity is measured when the retarding field analyzer voltage is set at 0 V.

DC (V)	10	40	50	80	100	120	150	160	200
m/z 69	970	2225	2026	1658					
m/z 131		86		285		1541		2536	3791
m/z 264			1401		1668		1420		1834
m/z 414			131		188		223		254
m/z 502			78		68		112		95

the coulombic repulsion in this experiment is different for each m/z ratio, which may explain why the q_z and a_z values at ejection are not aligned for all m/z ratios. However, ion abundance fluctuations did not cause any instability in the measurement of the ion ejection time, so the effect is probably not very significant.

Finally, there are several non-linear resonances that cross the $\beta_z = 0$ curve [30]. The ions may be ejected by non-linear resonance instead of crossing the $\beta_z = 0$ curve into an unstable zone of the stability diagram.

The general effect shown in Fig. 3 is that, when they are ejected from the QIT using a DC voltage on the ring electrode, ions are ejected at higher radiofrequency amplitudes than expected according to the stability diagram. However, the way in which the shift in the stability zone depends on the m/z ratio is not obvious. Therefore, we cannot tailor the increase in DC voltage on the ring electrode to the shape of the ejection time *vs.* m/z ratio in order to compensate for the time-of-flight dispersion in the transfer optics and to insure that all ions arrive simultaneously at the push–pull zone of the TOF analyzer. Working within the context of the Mathieu equations and the stability diagram is therefore not advantageous.

One important issue in an orthogonal QIT/TOF coupling is the efficiency of ion ejection and the kinetic energy of the ions when they are ejected from the QIT. Tables 1 and 2 show, for various values of the DC voltage, the evolution of the integrated ion signal and the kinetic energy distribution that was derived from it for the two ejection methods. The general trend for the total intensity of the ion signal (signal when there is no repulsion voltage) is to increase with the DC voltage for both ejection methods. This can be explained by the depth of the pseudo-potential well at ejection. Dehmelt et al. showed that, for low values of a_z and q_z, the depth of the pseudo-potential well increases along the q_z axis [28,31]. When the depth of the pseudo-potential well increases, the radius of the ion cloud decreases [32]. The number of ions ejected from the ion trap as opposed to the number of the ions hitting the exit end-cap electrode accordingly increases with q_z at ejection. Since the ejection q_z value increases with the DC voltage, the number of ejected ions increases with the DC voltage. Therefore, the ion signal increases, too. One notable exception is the evolution of the total ion intensity for m/z 69 when the DC voltage is applied to the ring electrode: in that case, a_z and q_z are both too high for Dehmelt's equations to apply.

Fig. 4 shows the kinetic energy distribution for m/z 414 using both methods of ion ejection. As can be expected, the kinetic energy of the ions increases when the DC voltage on the ring electrode or between the end-cap electrodes increases. We also notice that, for both methods, the kinetic energy distribution widens when the DC voltage increases and that the kinetic energy at the peak of the distribution is larger than the potential used to eject the ions from the QIT (since all the ions are singly charged, we took voltages in *V* to be equivalent to energies in *eV*). Although both ejection methods lead to wide kinetic energy distributions (the maximum kinetic energy is almost twice the voltage applied on the electrodes), the ejection efficiency of applying a voltage between the end-cap electrodes is much higher: comparison between the data in Tables 1 and 2 shows that, for equal voltages on the electrodes, the total ion intensity is much higher when the voltage is applied between the end-cap electrodes than when it is applied to the ring electrode. Again, this result is consistent with theory: when the ejection voltage is applied to the ring electrodes, ions can be ejected from the QIT towards both end-cap electrodes. However, when the DC voltage is applied between the end-cap electrodes, all ions are ejected in the direction of the same end-cap electrode (the one carrying the negative voltage). Therefore, the total ion intensity is expected to be higher when ions are ejected with a DC voltage between the end-cap electrodes than when ions are ejected with a DC voltage on the ring electrode.

In Figs. 5 and 6, we attempted to find out why the kinetic energy of the ions is so much higher than the DC voltages we applied to eject them from the QIT, since we did not observe any fragmentation occurring after ionisation. The shape of the signal, as seen in the insert of Fig. 3, suggested that ions were preferentially ejected when the RF voltage on the ring electrode was positive, and that, as a result, the RF amplitude could have an effect on the kinetic energy of the ions. For that purpose, we defined the extra kinetic energy carried by the fragment ions by the difference between the

Table 2
Total intensity of the ions ejected from the ion trap by application of a DC voltage between the end-cap electrodes. The total ion intensity is measured when the retarding field analyzer voltage is set at 0 V.

DC (V)	0	1	5	10	20	50
m/z 69		40	647	1130	1985	2932
m/z 131	118	566	1318	1901	3010	4094
m/z 264		55	259	373	718	758
m/z 414			116	140	267	371
m/z 502					45	69

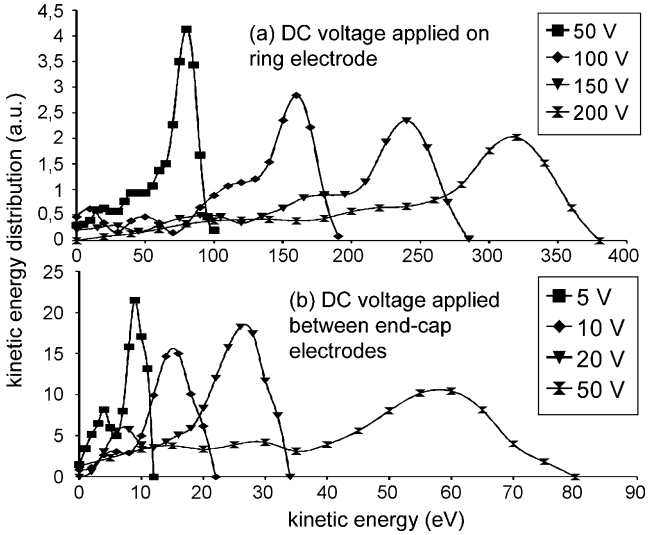

Fig. 4. (a) Kinetic energy distribution of m/z 414 by simultaneous radiofrequency shut-down and DC application on the ring electrode for several values of the voltage applied on the ring electrode. (b) Kinetic energy distribution of m/z 414 by simultaneous radiofrequency shut- down and DC application between the end-cap electrodes for several values of the voltage applied between the end-cap electrodes.

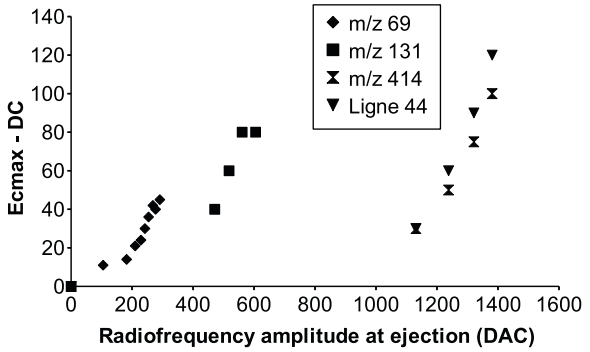

Fig. 5. Average kinetic energy due to the radiofrequency voltage vs. the amplitude of radiofrequency at ejection, for ions of various m/z ratios ejected by simultaneous shut-down of the radiofrequency and application of a DC voltage on the ring electrode. The average kinetic energy due to the radiofrequency voltage was calculated by subtracting the DC voltage on the ring electrode to the kinetic energy at the maximum of the kinetic energy distribution.

kinetic energy at the maximum of the distribution and the kinetic energy yielded by the DC voltage to an ion starting from the centre of the QIT. Figs. 5 and 6 show, for each ion species, the extra kinetic energy *vs*. the amplitude of the radiofrequency at ion ejection, which was calculated using the ejection time of each fragment ion species. We chose to express the voltage in DAC because that is the unit of radiofrequency amplitude in the QISMS software. The DAC unit is equivalent to $2\,V_{0-p}$. Regardless of the ejection method, the extra kinetic energy is proportional to the amplitude of the radiofrequency at ejection, which shows that the extra kinetic energy comes from the radiofrequency amplitude at ejection and is consistent with the idea that ions are preferentially ejected when the radiofrequency voltage is positive, as is suggested by the shape of the recorded signal (Fig. 3 insert). This result is also consistent with the results obtained by Reiser et al. [33] which show that the kinetic energy of ions ejected from the QIT increases with the radiofrequency amplitude. Figs. 5 and 6 show that, in both cases, the decrease of the radiofrequency amplitude is slow enough to let the ions follow the variation of the radiofrequency voltage: the stored ion cloud evolves adiabatically to its new state of stability.

The variation of the kinetic energy with the amplitude of the radiofrequency, however, is not identical for all ion species. We cannot conclude whether or not this variation depends on the m/z ratio, since other factors, like He pressure and coulombic repulsion, may come into play. We were also unable to explain the shape of the kinetic energy distribution, which, for each curve, differs significantly from the expected Gaussian-shaped curve.

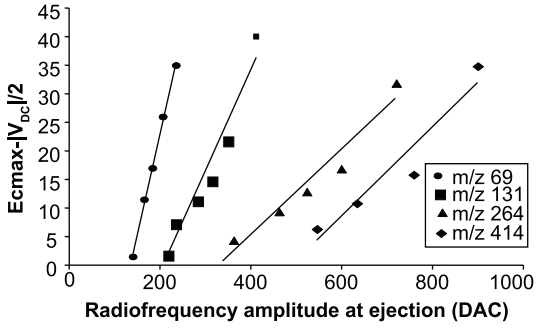

Fig. 6. Average kinetic energy due to the radiofrequency voltage vs. the amplitude of radiofrequency at ejection, for ions of various m/z ratios ejected by simultaneous shut-down of the radiofrequency and application of a DC voltage between the end-cap electrodes. The average kinetic energy due to the radiofrequency voltage was calculated by subtracting the voltage on the exit end-cap electrode to the kinetic energy at the maximum of the kinetic energy distribution.

For the purpose of coupling the QIT with a TOF analyzer, it is clear that ejecting the ions with a voltage on the end-cap electrodes is the best method of the two, because all the ions are directed to the exit end-cap electrode instead of being equally directed to each end-cap electrode. The negative potential on the exit end-cap electrode induces deceleration of the ions between the exit of the QIT and the acceleration zone of the TOF analyzer, which is at ground potential before the arrival of the ejected ion beam.

4. Conclusion

In this study, the behaviour of ions upon ejection from the QIT at low values of the q_z parameter of the stability diagram has been shown. We showed that the abundance of the ions successfully ejected from the QIT increases with the value of q_z at ejection, which is related to the pseudo-potential well depth. We also showed that the average kinetic energy of the ion cloud increases both with the ejection DC voltage, whether it is applied to the ring electrode or the end-cap electrodes, and the amplitude of the trapping voltage.

The abundance of the ejected ion cloud and its kinetic energy distribution are two conflicting influences when the QIT is used in a coupling with a TOF analyzer. On the one hand, it is important to eject ions at low kinetic energies, so that the mass spectra from the TOF analyzer are well-resolved. However, the overall instrument sensitivity depends on efficient ion ejection from the QIT and minimal ion loss during ion transfer from the QIT to the TOF push-pull zone. Our results show that it is necessary to compromise between ejecting ions at low voltages on the QIT electrodes to minimize ion kinetic energy, and at high enough voltage to maximize ion transmission and sensitivity. Therefore, it is important to measure the abundance and the kinetic energy of the ions at the ejection from the QIT before determining the properties (e.g., geometry, size, grids and applied potentials) of the TOF analyzer.

We chose these two ejection methods because they allow the ejection of ions in order of decreasing m/z ratios so that the time-of-flight dispersion in the transfer optics compensates the ejection time dispersion from the QIT. We refute the idea that the kinetic energy of the ions ejected from the QIT would not depend significantly on the m/z ratio and we show that the kinetic energy distribution of the ions depends on the amplitude of the RF voltage on the ring electrode at ejection time. Ions of different m/z ratios are ejected at different RF voltage amplitudes, and therefore have different kinetic energies. This affects their time of flight to the acceleration zone of the TOF analyzer.

This study shows that it is important, when building a coupling between a QIT and another analyzer, like the TOF analyzer, to carefully choose the method of ejection of the ions and the starting point of ejection of the ions in terms of the position in the stability diagram. The sensitivity and the resolving power of the final instrument will greatly depend on it.

Acknowledgements

The authors would like to thank Dr. Denis Lesage, Dr. Gareth Dobson and Dr. Jeremie Ponthus for helpful discussions. This work was financed with a grant from the Centre d'Etudes du Bouchet.

References

[1] R.E. March, J. Mass Spectrom. 32 (1997) 351–369.
[2] M. Guilhaus, J. Mass Spectrom. 30 (1995) 1519–1532.
[3] B.M. Chien, S.M. Michael, D.M. Lubman, Int. J. Mass Spectrom. Ion Process. 131 (1994) 149–179.
[4] U. Wilhelm, K.P. Aicher, J. Grotemeyer, Int. J. Mass Spectrom. Ion Process. 152 (1996) 111–120.
[5] V.M. Doroshenko, R.J. Cotter, J. Mass Spectrom. 33 (1998) 305–318.
[6] P. Kofel, M. Stöckli, J. Krause, U.P. Schlunegger, Rapid Commun. Mass Spectrom. 10 (1996) 658–662.

[7] Q. Ji, M.R. Davenport, C.G. Enke, J.F. Holland, J. Am. Soc. Mass Spectrom. 7 (1996) 10009–11017.
[8] F. Xian, J. Zhao, D.M. Lubman, J. Biomol. Tech. 18 (2007) 15–16.
[9] S.M. Michael, B.M. Chien, D.M. Lubman, Anal. Chem. 65 (1993) 2614–2620.
[10] P. Huang, X. Jin, Y. Chen, J.R. Srinivasan, D.M. Lubman, Anal. Chem. 71 (1999) 1786–1791.
[11] N. Goto-Inoue, T. Hayasaka, Y. Sugiura, T. Taki, Y.T. Li, M. Matsumoto, M. Setou, J. Chromatogr. B 870 (2008) 74–83.
[12] F. Zhang, Z. Jia, P. Gao, H. Kong, X. Li, J. Chen, Q. Yang, P. Yin, J. Wang, X. Lu, F. Li, Y. Wu, G. Xu, Talanta 79 (2009) 836–844.
[13] A.G. Marshall, C.L. Hendrickson, Annu. Rev. Anal. Chem. 1 (2008) 579–599.
[14] Y. Hashimoto, I. Waki, K. Yoshinari, T. Shishika, Y. Terui, Rapid. Commun. Mass Spectrom. 19 (2004) 221–226.
[15] Y. Hashimoto, H. Hasegawa, H. Satake, T. Baba, I. Waki, J. Am. Soc. Mass Spectrom. 17 (2006) 1669–1674.
[16] A. Favre, F. Gonnet, J.-C. Tabet, Rapid Commun. Mass Spectrom. 15 (2001) 446–450.
[17] G. Dobson, J. Murell, D. Despeyroux, F. Wind, J.-C. Tabet, Rapid Commun. Mass Spectrom. 17 (2003) 1657–1664.
[18] W.C. Wiley, I.H. McLaren, Rev. Sci. Instrum. 26 (1955) 1150.
[19] H.-P. Reiser, R.E. Kaiser, P.J. Savickas, R.G. Cooks, Int. J. Mass Spectrom. Ion Process. 106 (1991) 237–247.
[20] J.H.J. Dawson, M. Guilhaus, Rapid Commun. Mass Spectrom. 3 (5) (1989) 155–159.
[21] J.A. Simpson, Rev. Sci. Instrum. 32 (1961) 1283.
[22] H. Oomori, T. Kasuya, M. Wada, Y. Horino, N. Tsubouchi, Rev. Sci. Instrum. 71 (2000) 1122.
[23] Y. Cui, Y. Zou, A. Valfells, M. Reiser, M. Walter, I. Haber, R.A. Kishek, S. Bernal, P.G. O'Shea, Rev. Sci. Instrum. 75 (2004) 2736.
[24] R. Nachtrieb, B. LaBombard, E. Thomas, Rev. Sci. Instrum. 71 (2000) 4107.
[25] R.A. Pitts, R. Chavan, S.J. Davies, S.K. Erents, G. Kaveney, G.F. Matthews, G. Neill, J.E. Vince, JEFF-EFDA Contributors, I. Duran, Rev. Sci. Instrum. 74 (2003) 4644.
[26] S. Catinella, P. Traldi, X. Jiang, F.A. Londry, R.J.S. Morrison, R.E. March, S. Grégoire, J.-C. Mathurin, J.-C. Tabet, Rapid Commun. Mass Spectrom. 9 (1995) 1302–1309.
[27] C. Marinach, A. Brunot, C. Beaugrand, G. Bolbach, J.-C. Tabet, Int. J. Mass Spectrom. 213 (2002) 45–62.
[28] J.F.J. Todd, R.M. Waldren, R.E. Mather, Int. J. Mass Spectrom. Ion Phys. 34 (1980) 325–349.
[29] S. Grégoire, J.-C. Mathurin, R.E. March, J.-C. Tabet, ICR/Ion Trap Newsletter 43 (1996) 12.
[30] D.M. Eades, J.V. Johnson, R.A. Yost, J. Am. Soc. Mass Spectrom. 4 (1993) 917–929.
[31] H.G. Dehmelt, Adv. At. Mol. Phys. 3 (1967) 53.
[32] S. Guan, A.G. Marshall, J. Am. Soc. Mass Spectrom. 5 (1994) 64–71.
[33] H.P. Reiser, R.E. Kaiser, P.J. Savickas, R.G. Cooks, Int. J. Mass Spectrom. Ion Process. 106 (1991) 237–247.